A Coupled Aero-Structural Optimization Method For Complete Aircraft Configurations

James J. Reuther*
MCAT Institute

Juan J. Alonso†
Stanford University

Joaquim R. R. A. Martins‡
Stanford University

Stephen C. Smith§
NASA Ames Research Center

1 Abstract

This paper presents a new framework for the coupled optimization of aero-structural systems. The framework permits the use of high-fidelity modeling of both the aerodynamics and the structures and represents our first step in an effort towards the development of a high-fidelity multidisciplinary optimization capability. The approach is based on efficient analysis methodologies for the solution of the aerodynamics and structures subproblems, an adjoint solver to obtain aerodynamic sensitivities, and a multiprocessor parallel implementation. We have placed a geometry database representing the outer mold line (OML) of the configuration of interest at the core of our framework. Using this geometry description, the information exchange between aerodynamics and structures is accomplished through an independent coupling of each discipline with the OML database. The framework permits the later inclusion of other disciplines, such as heat transfer and radar signatures, with relative ease. Specific results from the coupling of a finite volume flow solver for the Euler and Reynolds Averaged Navier-Stokes equations with two different linear finite element structural models are explored. Care is taken in the treatment of the coupling of the disciplines such that a consistent and conservative scheme is achieved. Direct comparisons with wind-tunnel data are presented to demonstrate the importance of aeroelastic solutions. In addition, simplified design examples are presented to illustrate the possible advantages of the new aero-structural design methodology in evaluating trade-offs between aerodynamic performance and structural weight for complete aircraft configurations.

2 Introduction

Considerable research has already been conducted on the multidisciplinary optimization (MDO) of flight vehicles. The survey paper by Sobieski [1] provides a comprehensive discussion of much of the work completed to date. These efforts have ranged from the development of techniques for discipline coupling to actual demonstrations on real-world design problems. In most cases, these research efforts have shown the importance of interdisciplinary coupling, as well as the inability of sequential disciplinary optimization to achieve the true global optimum of a coupled system. For example, Wakayama [2, 3] has shown that in order to obtain realistic planform shapes in the design of aircraft configurations it is necessary to include both multiple disciplines and a complete set of real-world constraints. Meanwhile, in the design of novel configurations such as a joined-wing aircraft, Gallman [4] demonstrated that only multidisciplinary methods are capable of revealing the relevant design trade-offs; single-discipline optimization often leads to incorrect design choices. Unfortunately, the

*AIAA Member, Research Scientist, NASA Ames Research Center, MS 227-6, Moffett Field, CA 94035, U.S.A.

†AIAA Member, Assistant Professor, Department of Aeronautics and Astronautics, Stanford University, Stanford, CA 94305, U.S.A

‡AIAA Student Member, Graduate Student, Department of Aeronautics and Astronautics, Stanford University, Stanford, CA 94305, U.S.A

§AIAA Member, Research Scientist, NASA Ames Research Center, MS 227-6, Moffett Field, CA 94035, U.S.A.

fidelity in the modeling of the various component disciplines in these preliminary design tools has remained at a relatively low level. Therefore, while useful at the conceptual design stage, these tools cannot accurately represent a variety of nonlinear phenomena, such as wave drag, which can play a key role during the detailed design phase.

On the other hand, recent applications of aerodynamic shape optimization using high-fidelity CFD methods have resulted in substantial improvements in the aerodynamic performance of complex aircraft configurations [5, 6, 7, 8, 9]. Jameson, et al. [10, 11, 12, 13, 14] have developed a mathematical framework for the control of systems governed by the Euler and Navier-Stokes equations that has resulted in significant reductions in the computational cost of aerodynamic shape optimization (ASO). Despite the broad possibilities that these new ASO methods have brought about, they also have had their share of problems. In the case of aerodynamic wing design, planform and thickness constraints have often been artificially imposed so that structural weight, fuel volume, and takeoff/landing requirements would not be adversely affected by the changes in the wing shape. These constraints were typically guided by the result of low-fidelity multidisciplinary models and individual decisions made by experts from selected disciplines. By neglecting the coupling between various disciplines, design constraints have often been too restrictive to permit significant performance improvements, or not restrictive enough, thus allowing ASO to produce infeasible designs. In addition, improvements in aerodynamic performance resulting from span load changes cannot be accurately quantified in view of their unknown impact on the structural weight.

Enabled by recent advances in single-discipline optimization, novel restructuring of the multidisciplinary design process [15, 16], and affordable supercomputing alternatives [17, 9], the opportunity now exists to develop an MDO framework which allows the participation of various relevant disciplines with high-fidelity modeling. The goal here is not to use high-fidelity modeling to construct a response surface [18] or train a neural network [19] but to use it directly during design. This kind of MDO environment has yet to be developed, but promises to improve upon existing design methodologies by increasing the level of confidence in the final results from preliminary design. A higher confidence level at an earlier stage in the design process holds out the possibility of dramatically reducing the development costs of the detailed design phase. Furthermore, the overall quality and performance of the resulting design will be improved when compared with traditional sequential design strategies.

The goal of the current research is to establish a new framework for high-fidelity MDO. The important contributions presented to support such a framework are:

- The use of high-fidelity modeling of two disciplines (RANS aerodynamics and linear FEM structures).
- An OML geometry database which serves as both an interface to the optimization algorithm and an interface for communication between disciplines.
- Sophisticated coupling algorithms that link each discipline to the OML such that information transfer between the disciplines is consistent and conservative.
- A framework for the computation of coupled sensitivities.

An excellent demonstration problem which illustrates the strong coupling that can occur between disciplines is the case of aeroelastic wing design. The optimized shape and structure are the result of compromises among numerous requirements and constraints. Changes in the span load may lead to improvements in induced drag but they can also incur a structural weight penalty. Similarly, an increase in the thickness-to-chord ratio of the wing sections may substantially improve the structural efficiency of the configuration, but it may also lead to an undesirable increase in compressibility drag. Moreover, design constraints are often set by off-design conditions, such as protection from high-speed pitch-up, leading to the need to simulate these conditions as well.

The complete aero-structural design problem involves the simultaneous optimization of the aerodynamic shape of a configuration and the structure that is built to support its loads. The cost function to be optimized requires a combination of aerodynamic performance and structural weight, in order to address two of the main components of the Breguet range equation. Design variables are set up to parameterize the external aerodynamic shape of the configuration and the shape and material properties of the underlying structure (spar cap areas, skin thicknesses, etc.). The design problem must also impose various constraints on the details of the structure, such as the yield stress criterion (the maximum stress in any part of the structure may not exceed the yield stress of the material at a number of critical load conditions with the appropriate safety margin), minimum skin thickness constraints, and fuel volume requirements. On the aerodynamics side, equality and inequality constraints may be imposed on both the total lift and pitching moment. Details of the pressure distribution for a transonic wing design problem, such as the location of the upper surface shock, the slope of the pressure recovery,

and the amount of aft loading, may also be imposed as design constraints.

The desired high-fidelity MDO framework for flight vehicle design suggested by this work must address the following issues:

1. Level of accuracy of disciplinary models.
2. Coupling between disciplines.
3. Computation of sensitivities.

In order to obtain the necessary level of accuracy, we intend to use high-fidelity modeling for both the aerodynamic and structural subsystems. For this purpose, an Euler and Reynolds Averaged Navier-Stokes (RANS) flow solver has been used to model the aerodynamics. The details of the multiblock solver, FLO107-MB, can be found in Ref. [7] and its parallel implementation on a variety of computing platforms has been described in Ref. [9, 17]. Two different Finite Element Methods (FEM) have been used for the description of the behavior of the structure. The first is a linear FEM model that uses brick elements which are appropriate for solid wind tunnel configurations. The second is a linear FEM that uses truss and triangular plate elements to model the structural components of aircraft configurations. Given these choices of the physical models for the disciplines involved, it will be possible to capture all of the key trade-offs present in the aero-structural design problem.

In our work, the inter-disciplinary coupling is performed using a geometry database of the outer mold lines (OML). All exchanges of information between disciplines are accomplished by independent communication with this OML database. This has the advantage of standardizing the communication process and facilitates the inclusion of other disciplines. For the specific case of aero-structural coupling, we have chosen to follow the work of Brown [20] in order to carry out the bidirectional transfer of loads and displacements between the structure and the CFD mesh via the OML database. Careful attention has been paid to the consistency and conservativeness of the load transfer, to the point that we believe the current setup will be suitable even for unsteady aeroelastic flutter analysis. A consistent transfer is one that preserves the resultant forces and moments. If, in addition, the total work and energy are conserved, the transfer method is said to be conservative.

The strong interdependence between aerodynamics and structures makes the computation of sensitivities of cost functions and constraints a difficult task. In our past works, we have obtained the sensitivities of aerodynamic cost functions using the solution of an adjoint equation. This technique produced aerodynamic sensitivities at a fraction of the cost of traditional methods such as the finite-difference approach. The advantage of using the adjoint approach was due, in large part, to the fact that the number of design variables was much larger than the number of functions for which sensitivities were needed.

In the case of combined aero-structural design, a similar approach can be pursued: a set of aero-structural adjoint equations can be formulated which considerably reduce the cost of coupled sensitivity analysis. However, the nature of the aero-structural design problem is such that the number of design variables is not always larger than the number of cost functions and constraints. In particular, this problem is often characterized by a large number of structural stress constraints (one per element in the complete finite element model). Thus, by using a coupled adjoint approach directly it will be necessary to calculate a separate adjoint system for each of these structural constraints. The straightforward alternative to the adjoint approach is to use finite differencing. For cases in which the number of design parameters is relatively small, this alternative may indeed prove more cost-effective. However, the desired goal of admitting a large number of design variables makes the computational cost of the finite-difference approach unaffordable. Similarly problematic is the use of the "direct" approach often used efficiently in structural optimization. A prefactored CFD Jacobian matrix is simply too large to compute with reasonable resources. Given these constraints, the sensitivity analysis aspect of high-fidelity MDO will require much further future research. Details of the simplified sensitivity analysis used here, as well as a framework to obtain coupled sensitivities, are presented in Section 5.3.

3 Structural Finite Element Models

In order to allow for the possibility of utilizing an arbitrary finite element model for the description of the structure, a detailed Application Programming Interface (API) has been developed. This API explicitly outlines both the content and format of the information that must be provided by a Computational Structural Mechanics (CSM) solver intended for aeroelastic design. The API definition has also been kept general enough to allow for a variety of element types within the same model.

The integration of existing and future structural solvers with the design code is therefore accomplished through the use of this API. A typical sequence of calls to the structural model is as follows: the first function call in the API consists of an initialization process that builds the structural model and all ancillary arrays, matrices, and matrix de-

compositions. Additional functions in the API provide the design algorithm with the complete geometry description of the external surface of the structural model and the interpolation functions for both the coordinates and displacements at any point of the structural model surface. Simple function calls exist in the API to obtain the structural displacement vector and a list of element principal stresses. Finally, since the design module continuously updates the OML geometry, an additional API call is used to update the structural model geometry and its stiffness matrix such that they conform to the OML.

For the results presented in this paper, we chose to develop our own CSM solvers so that any necessary changes to the source code could be made readily. Retrospectively, it became clear that once a coupling interface was defined, no source code for the CSM solver needed to be examined. The only adaptation to existing CSM methods that will be required is the creation of a conforming interface (see Section 4). Thus, in future works we intend to couple the same MDO framework with commercially available CSM codes such as ANSYS and MSC-NASTRAN. The two CSM solvers developed here use different finite element types and meshing strategies. They were built to reflect accurately the behavior of the types of wing structures present both in wind tunnel models and in real aircraft. Both solvers require the solution of the classical structural equilibrium equation,

$$\mathbf{Kq} = \mathbf{f}. \tag{1}$$

Here, $\mathbf{K}$ is the global stiffness matrix of the structure, $\mathbf{q}$ is the vector of nodal displacements, and $\mathbf{f}$ is the vector of applied nodal forces. With the appropriate boundary conditions, matrix $\mathbf{K}$ is symmetric and non-singular. For the problem sizes of interest here, a Cholesky factorization is appropriate. This factorization can be stored and used multiple times with changing load vectors during an aeroelastic calculation. The stresses in each element can then be related to the displacements by the following equation:

$$\sigma = \mathbf{Sq}, \tag{2}$$

where $\mathbf{S}$ represents the product of the constitutive law matrix, the nodal displacement-strain matrix and the local-to-global coordinate transformation matrix.

3.1 Wind Tunnel Model CSM Solver

A simple CSM solver was developed to compute deflections of wind tunnel model wings. Because wind tunnel models are typically machined from a single billet, 8-node isoparametric hexahedral solid elements were chosen to represent this type of solid structure. These "brick" elements have 24 degrees of freedom, representing the 3 components of the displacement at each node. The stiffness matrix for each element is found using an 8-point (2 points in each coordinate direction) Gauss quadrature of the strain energy distribution within the element. These elements are called "isoparametric" because the same interpolation functions are used to describe the displacement field and the metric Jacobians used for the global coordinate transformation.

The CSM solver was designed to exploit the convenience of an ordered arrangement of elements; element connectivity is implied by the point ordering of the input CSM mesh. This approach greatly simplifies input, and allows the flexibility of modeling the channels typically cut in the wing surface to install pressure orifices and route pressure tubing. For this purpose, finite element nodes can be located along the channel edges, so that distinct brick elements occupy the volume of the pressure channels. The modulus of elasticity is then set to zero for these elements, thus simulating the missing material.

For this study, the geometries of two typical business jets were chosen since wind tunnel measurements and CFD computational meshes were already available in both cases. For each of the wings, a finite element model was constructed using 8-node brick elements. To avoid zero-height elements at the leading and trailing edges, the wing surface definition was truncated at 4% and 96% of the wing chord. The motion of all nodes at the side of the fuselage is fully constrained. The remaining enclosed volume was modeled by an ordered mesh of 4 nodes through the wing thickness, 6 nodes in the chordwise direction, and 44 nodes spanwise from the side of the fuselage to the wing tip. For both cases, this results in 645 elements and $3,168$ degrees of freedom. A typical wing CSM mesh is shown in Figure 1 together with the location of the points on the surface of the OML and short segments indicating the points on the CSM surface from which the OML derives its displacements.

3.2 Aircraft Structure CSM Solver

A different CSM solver was used to model the behavior of realistic aircraft structures. This solver models a wing with multiple spars, shear webs, and ribs located at various spanwise stations, and the skins of the upper and lower surfaces of the wing box. The structural solver is based on a finite element code, *FESMEH*, developed by Holden [21] at Stanford.

Two types of finite elements are used: truss and triangular plane-stress plate elements. Both element types have 3 translational degrees of freedom per node, so the truss has a total of 6 degrees of freedom and the plate has 9 degrees of freedom. Figure 2 shows a graphical representation of these two element types. Neither of these elements can carry

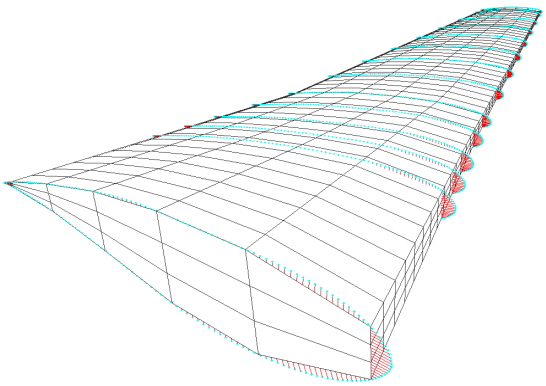

Figure 1: Brick-element mesh of wind tunnel model wing.

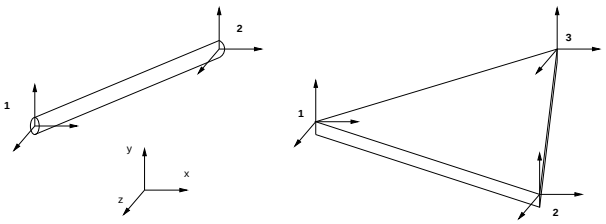

Figure 2: Truss and Triangular Plane Stress Plate elements

a bending moment, since their nodes do not have rotational degrees of freedom. The wing bending, however, is still well-captured since the contributions of the second moments of inertia for the plates and trusses due to their displacement from the wing neutral axis is dominant when compared to their individual moments of inertia about their own neutral axes. The only limitation when using these kinds of elements is that each of the nodes must be simply supported, implying that we can have only one set of plate elements between any two spars.

In the modeling of a typical wing structure, triangular plates are used to model the wing skins. Plates are also used for the shear webs of spars and ribs, while the upper and lower spar caps are modeled using trusses. The wing model in our case consisted of 6 spars and 10 ribs, adding up to a total of 132 nodes and 640 elements. Figure 3 shows the geometry of the finite element discretization used.

4 Aero-Structural Coupling Techniques

Within the framework described previously, the optimization of aero-structural systems requires, at least, the solution of the coupled aeroelastic analysis problem. The interaction between these two disci-

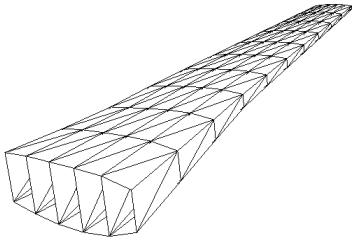

Figure 3: Wing Structural Model

plines, aerodynamics and structures, is quite strong since the former provides the necessary loads to the latter in order to determine the displacement field of the structure. In return, the structure provides surface deflections that change the aerodynamic properties of the initial configuration.

Two issues in this transfer of information between disciplines are of utmost importance to the success of an automatic design technique: first, the level of fidelity in the coupling of both disciplines has to be carefully considered in order to guarantee that the accuracy of the individual disciplines is not jeopardized, and second, the evolving disciplinary designs must have exact geometric agreement by the end of the design process.

In order to tackle the fidelity of the coupling, we have chosen to ensure that the transfer of the distributed pressure forces and moments from the CFD calculation to the CSM nodal load vector is both consistent and conservative as defined in the approach developed by Brown [20]. The property of consistency implies that the resultant forces and moments imparted by the distributed pressure field, p, must be equal to the sum of the nodal forces and moments in the CSM load vector, $\mathbf{f}$. Conservation addresses the important issue that the virtual work performed by the load vector, $\mathbf{f}$, undergoing a virtual displacement of the structural model (represented by $\delta\mathbf{q}$) must be equal to the associated work performed by the distributed pressure field, p, undergoing the associated displacement of the CFD mesh surface, $\delta\mathbf{r}$. Thus, a procedure is devised that describes the motion of every surface point in the CFD mesh as a function of the nodal displacements of the structural model,

$$\delta\mathbf{r} = [\eta]^T \cdot \delta\mathbf{q}, \tag{3}$$

where $[\eta]$ is a matrix of linear weights on the displacement vector that is a combination of interpolations within the CSM mesh and extrapolations to the OML as described by Brown [20]. The virtual work in the CSM model can be represented as

$$\delta W_{CSM} = \mathbf{f}^T \cdot \delta\mathbf{q},$$

while the virtual work performed by the fluid acting

on the surface of the CFD mesh is given by

$$\delta W_{CFD} = \int_{\partial\Omega} p\, \mathbf{n}^T \cdot \delta\mathbf{r}\, dS + \int_{\Omega} \mathbf{b}^T \cdot \delta\mathbf{r}\, dV.$$

Here, $\mathbf{b}$ represents a distributed body force per unit mass, if it exists, and $\partial\Omega$ is the CFD mesh surface that describes the interface between the fluid and the structure. For a conservative scheme, $\delta W_{CFD} = \delta W_{CSM}$, and the consistent and conservative load vector is given by:

$$\mathbf{F}^T = \int_{\partial\Omega} p\, \mathbf{n}^T \cdot [\eta]^T\, dS + \int_{\Omega} \mathbf{b}^T \cdot [\eta]^T\, dV. \qquad (4)$$

For the two different structural models used in this work, the procedure used to obtain the relation in Eq. 3 is implemented in a preprocessing step following Brown's approach. The matrix $[\eta]$ is thus precomputed and stored for later use during the aeroelastic iteration procedure and plays a key role in both the transfer of displacements and the computation of the conservative and consistent load vector.

In order to enable communication between the aerodynamic and structural solvers, a standardized OML surface representation of the configuration of interest is required. Solutions from each of the disciplines (aerodynamics and structures) are interpolated onto this OML database so that they may be accessed as needed by the other disciplines.

For this purpose, the OML geometry produced by *AeroSurf* has been used as the central database. *AeroSurf* is a geometry generation system that has been specifically created for the analysis and design of aircraft configurations including fuselage, wings, pylons, nacelles, and empennage [5, 6]. *AeroSurf* preserves an aerodynamic geometry component view of the complete configuration. These geometry components are stored un-intersected in three-dimensional space. Typically, aerodynamic shape changes are applied to these un-intersected components, and, once all modifications are completed, a new configuration is created by finding the intersection(s) of the resulting surfaces. The intersected geometry is then decomposed into a series of well-defined parametric patches that constitute the OML of the complete configuration. These patches (or the points they are composed of) serve as the interface between aerodynamic and structural calculations. It is our intention to expand the capability of this geometry-based interface to include additional disciplines in the future.

Each *AeroSurf* point is associated with a point on the surface of the CSM model in a preprocessing step. During optimization, the displacements of each *AeroSurf* point are calculated by first using the CSM basis functions to interpolate the CSM nodal displacements at the projected *AeroSurf* point. Then extrapolation functions are used to carry the displacements from the CSM mesh to the OML. When the CSM solver dictates a new position for the structure, the locations in three-dimensional space of all the *AeroSurf* points are updated by adding the deflections to the jig-shape points. This update process effectively constructs new parametric patches to represent the surface of the perturbed configuration. In a similar fashion, during a preprocessing step, every point on the surface of the CFD mesh is associated with an *AeroSurf* patch and a parametric location within that patch. The CFD points are assumed to be "tied" to these parametric locations, and, when the *AeroSurf* database is altered, the location of the CFD surface mesh points can be obtained by straightforward evaluation of their parametric locations on the corresponding *AeroSurf* patches. As can be seen, *AeroSurf* plays a central role in the transfer of displacements from CSM to CFD.

Furthermore, the *AeroSurf* database also plays a similar role in the transfer of pressure information from the CFD calculation to the structural load vector. The transfer of surface pressure information to the *AeroSurf* database is achieved by identifying the "donor" cells from the CFD mesh that contain the desired information. The pressure integrations in Eq. 4 are then performed with the same accuracy as can be achieved if the integration were to occur directly on the surface of the CFD mesh. The underlying assumption is that the mesh resolution of the *AeroSurf* database is comparable to, if not better than, that of the CFD surface mesh. This has always been the case in our design efforts. The coupling between aerodynamic and structural solvers in order to obtain an aeroelastic solution is achieved in an explicit, sequential, iterative fashion by exchanging information at regular intervals during the convergence process. This coupling is greatly simplified by the fact that only static aeroelastic solutions are considered in this work, and the issue of time accuracy is inconsequential. For a typical complete, rigid configuration at fixed lift, an Euler solution requires in the neighborhood of 120 multigrid cycles to reduce the average density residual by 5 orders of magnitude. It has been found that, for fixed-lift aeroelastic calculations, the number of multigrid iterations required increases by at most 10% if information is exchanged between the structural model and the aerodynamics every 10 multigrid cycles. Of course, in addition to the larger number of iterations required, the cost of the structural solution has to be accounted for. However, most of this cost is incurred in the decomposition of the stiffness matrix, and, as mentioned above, this can be accomplished in a preprocessing step. During the process of an update to the structures, all that remains to be done is the creation of a load vector and a back-solve operation with the already factored stiffness matrix.

The *AeroSurf* geometry database is currently a set of subroutines which are compiled together with the main optimization program. As the number of disciplines increases, a desirable development would be to make the OML database a stand-alone program that communicates directly with all the participating disciplines. The *AeroSurf* OML can then take the form of a daemon, and all communication can be made via sockets.

Finally, although the current implementation of *AeroSurf* relies on geometry creation and manipulation routines that we have developed, the ultimate goal is to use *AeroSurf* as a front-end to a Computer Aided Design (CAD) geometry kernel. This would greatly facilitate the transfer of information back to the working engineering model once the objectives of the design have been met. An interesting possibility is to use the Computational Analysis PRogramming Interface (CAPRI) developed by Haimes [22] which enables individual discipline programs to interact *directly* with a CAD solid model representation of the geometry in question. However, even in this CAD-oriented scenario, the process of component-based design with the necessary re-intersections will still form the core of the methodology.

5 Sensitivity Analysis

The proposed high-fidelity MDO framework will also need a strategy to perform design changes in a way that will minimize the need for expensive function evaluations. Detailed shape optimization of aerodynamic surfaces for transonic wing design problems requires a parameter space of $\mathcal{O}(100)$ or larger [23, 24]. This requirement combined with the enormous cost of each function evaluation renders the use of zeroth-order methods, such as random searches and genetic algorithms, inefficient for this problem. The alternative of using a response surface whereby a polynomial fit of the design space is constructed prior to optimization is also plagued with intractable computational costs since the number of function evaluations required is proportional to the square of the number of design variables.

If we assume that the basic topology of the structure (i.e., the number of spars, the number of ribs, the choice of materials, etc.) is not altered during the design, the design space should be smooth. Although many alternative global optimization strategies exist, for the aero-structural problem of interest, a gradient-based procedure holds the most promise. Gradient-based optimization algorithms can be shown to converge only to a local optimum. If the cost function of the aero-structural problem is sufficiently multi-modal, these algorithms can fail to achieve the global optimum. Nevertheless, when used in conjunction with lower-fidelity MDO tools that provide a reasonable starting point for the optimization, they can yield significant and credible improvements in the design.

When compared with zeroth-order methods, gradient-based algorithms shift the computational burden from evaluating the cost function to calculating values of its gradient. The most direct way to estimate gradients is the finite-difference approach in which a separate function evaluation is required for each design variable in the problem. By using gradient information, the total number of function evaluations is greatly reduced. However, given the large computational cost involved in each function evaluation, the finite-difference method has proven to be unaffordable for the aerodynamic design of complete configurations. This limitation of the finite-difference method has provided the motivation to develop new methods of obtaining sensitivity information for aerodynamic design problems. In particular, the control theory adjoint technique has proven extremely valuable in making these kinds of calculations possible.

5.1 Aerodynamic Sensitivities

The ground-breaking development of the adjoint methodology for both the Euler and Navier-Stokes equations was pioneered by Jameson [13, 14, 12, 10]. Its extensions to treat complex configurations including the treatment of linear and non-linear constraints and mesh deformations has been demonstrated by the first author [5, 6, 9].

In essence, the adjoint approach is able to obtain the gradient of a cost function with respect to an arbitrary number of design variables through the solution of a co-state equation. Given an aerodynamic cost function, I, which depends on both the flow field variables, $\mathbf{w}$, and the physical location of the OML boundary, $\mathcal{F}$,

$$I = I\left(\mathbf{w}, \mathcal{F}\right),$$

a change in $\mathcal{F}$ results in a change

$$\delta I = \frac{\partial I^T}{\partial \mathbf{w}} \delta \mathbf{w} + \frac{\partial I^T}{\partial \mathcal{F}} \delta \mathcal{F} \tag{5}$$

in the cost function. The governing equation, R, and its first variation express the dependence of $\mathbf{w}$ and $\mathcal{F}$ within the flow field domain:

$$R\left(\mathbf{w}, \mathcal{F}\right) = 0, \quad \delta R = \left[\frac{\partial R}{\partial \mathbf{w}}\right] \delta \mathbf{w} + \left[\frac{\partial R}{\partial \mathcal{F}}\right] \delta \mathcal{F} = 0. \tag{6}$$

Next, introducing a Lagrange multiplier, ψ, we have

$$\begin{aligned} \delta I &= \tfrac{\partial I^T}{\partial \mathbf{w}} \delta \mathbf{w} + \tfrac{\partial I^T}{\partial \mathcal{F}} \delta \mathcal{F} - \psi^T \left(\left[\tfrac{\partial R}{\partial \mathbf{w}}\right] \delta \mathbf{w} + \left[\tfrac{\partial R}{\partial \mathcal{F}}\right] \delta \mathcal{F} \right) \\ &= \left\{ \tfrac{\partial I^T}{\partial \mathbf{w}} - \psi^T \left[\tfrac{\partial R}{\partial \mathbf{w}}\right] \right\} \delta \mathbf{w} + \left\{ \tfrac{\partial I^T}{\partial \mathcal{F}} - \psi^T \left[\tfrac{\partial R}{\partial \mathcal{F}}\right] \right\} \delta \mathcal{F}. \end{aligned} \tag{7}$$

Choosing ψ to satisfy the adjoint or co-state equation

$$\left[\frac{\partial R}{\partial \mathbf{w}}\right]^T \psi = \frac{\partial I}{\partial \mathbf{w}}, \tag{8}$$

the first term in Eq. (7) is eliminated, and we find that the desired gradient is given by

$$\mathcal{G}^T = \frac{\partial I^T}{\partial \mathcal{F}} - \psi^T \left[\frac{\partial R}{\partial \mathcal{F}}\right]. \tag{9}$$

Since Eq. (9) is independent of $\delta\mathbf{w}$, the gradient of I with respect to an arbitrary number of design variables can be determined without the need for additional flow field evaluations. The main cost incurred is in solving the adjoint equation. In general, the complexity of the adjoint problem is similar to that of the flow solution. If the number of design variables is large, it becomes compelling to take advantage of the cost differential between one adjoint solution and the large number of flow field evaluations required to determine the gradient using finite differences. Once the gradient is obtained, any descent procedure can be used to obtain design improvements. At the end of each optimization iteration, new flow and adjoint calculations are performed to obtain an updated gradient, and the process is repeated until the cost function reaches a minimum.

It must be noted that in the case of aerodynamic design it is often the case that the problems are characterized by a large number of design variables and a small number of independent aerodynamic cost functions and constraints. This ratio of design variables to cost functions and constraints is often the opposite in structural optimization problems. If an aerodynamic problem were characterized by having a larger number of aerodynamic constraints compared with the number of design variables, the finite difference approach may be more suitable. The alternative *direct* approach, often used for structures, requires the solution of

$$\left[\frac{\partial R}{\partial \mathbf{w}}\right] \delta\mathbf{w} = -\left[\frac{\partial R}{\partial \mathcal{F}}\right] \delta\mathcal{F} \tag{10}$$

for $\delta\mathbf{w}$, followed by a substitution into Eq. (5). It is noted that $\delta\mathbf{w}$ must be calculated for each design variable independently. For small problems, it is possible to factor and store $\frac{\partial R}{\partial \mathbf{w}}$ and obtain all the $\delta\mathbf{w}$ vectors by a series of back-substitutions [25]. Unfortunately, for large three-dimensional Euler and Navier-Stokes problems, the cost of factoring $\frac{\partial R}{\partial \mathbf{w}}$ is not acceptable, leaving the advantage of the direct approach difficult to obtain. For many flow regimes of interest, the linearization of the CFD Jacobian matrix introduced in Eq. (10) is an unacceptable approximation. Most aerodynamic solvers make no attempt to compute the Jacobian matrix; it is simply too large and prefactoring it does not yield the advantage seen for linear systems. Thus, without prefactoring, the cost of solving Eq. (10) for each design variable is not too different from the cost of finite differencing.

The reader is referred to our earlier works for the detailed derivation of the adjoint equations specific to either the Euler or Navier-Stokes equations as well as the other elements necessary to create an overall design algorithm [5, 6, 9].

5.2 Structural Sensitivities

In the structural optimization subproblem, typical design variables include the cross-sectional areas of the truss elements that are used to model the spar caps, and the thicknesses of the plate elements that model the shear webs and skins.

The functions for which we require sensitivity information will typically be the total weight of the structure and the maximum stress on a given element. These are used as part of the overall cost function (aerodynamic performance plus structural weight) and to impose constraints on the problem. The sensitivities of the total weight with respect to the element size are trivial, since the weight of a given element is proportional to a given dimension. The sensitivities of the element stresses can be calculated in a straightforward fashion using finite differences. However, this approach is not very cost-effective since it requires the assembly and factorization of the global stiffness matrix, along with the solution of the structural equilibrium equation for each of the design variables. Although the finite-difference method was used in the results presented in this work, the method of choice is the *direct method* which is more efficient for cases where the number of cost functions and constraints is larger than the number of design variables [26]. For cases in which the number of design variables dominates the problem, a structural adjoint method analogous to the aerodynamic adjoint method can be used.

In the following, we are interested in obtaining the sensitivity of a vector-valued function g_i, $(i = 1, \ldots, n_{elems})$ to the design parameters $\mathcal{P}$. In other words, we are seeking the values for all the entries in the matrix $\left[\frac{dg_i}{d\mathcal{P}}\right]$, where the cost function, say structural weight, is but a single component of g_i.

The *direct method* is derived by taking the first variation of Eq. (1):

$$\mathbf{K}\,\delta\mathbf{q} = \frac{\partial \mathbf{f}}{\partial \mathbf{q}}\,\delta\mathbf{q} - \frac{\partial \mathbf{K}}{\partial \mathcal{P}}\,\mathbf{q}\,\delta\mathcal{P} + \frac{\partial \mathbf{f}}{\partial \mathcal{P}}\,\delta\mathcal{P}. \tag{11}$$

It must be noted that for static load conditions, where the load vector is assumed to be independent of the structural design variables and deflections, as is often the case for structural optimization as a single discipline,

$$\frac{\partial \mathbf{f}}{\partial \mathcal{P}} = 0, \quad \text{and} \quad \frac{\partial \mathbf{f}}{\partial \mathbf{q}} = 0. \tag{12}$$

This reduces Eq. (11) to

$$\mathbf{K}\ \delta\mathbf{q} = -\frac{\partial \mathbf{K}}{\partial \mathcal{P}}\ \mathbf{q}\ \delta\mathcal{P}. \tag{13}$$

As is shown later, the assumption of a constant load vector does not hold in the more general problem of coupled aeroelastic design.

To find $\delta\mathbf{q}$, Eq. (13) can be solved using the previously factorized stiffness matrix by the same method used for the solution of Eq. (1). This procedure needs to be repeated for each design variable.

To obtain the sensitivity of a vector of functionals g_i (where g_i could represent the stress in an element in addition to any cost functions), we write the total variation with respect to the design variables as follows:

$$\delta g_i = \frac{\partial g_i}{\partial \mathcal{P}}\ \delta\mathcal{P} + \frac{\partial g_i}{\partial \mathbf{q}}\ \delta\mathbf{q}. \tag{14}$$

Note that $\delta\mathbf{q}$ is valid for the evaluation of the sensitivity of any functional.

It is seen that the prefactored stiffness matrix renders the solution with respect to a significant number of design variables relatively inexpensive. In the work presented for this paper, where the cost of the aerodynamic state and co-state analyses are at least 2 orders of magnitude more than that of the structural analyses, the benefit of using the direct approach has not as yet been pursued.

5.3 Coupled Sensitivities

The computation of sensitivities for the aero-structural problem has components of both ASO and structural optimization techniques. However, if the true sensitivities of the design problem are needed, the coupling terms cannot be neglected. For example, the sensitivity of the stress in a given element of the CSM model to an aerodynamic twist variable has a component that depends on the change to the geometry of the structural model and a second component that depends on the changing load vector applied to the structure. Both of these contributions are significant and must be accounted for. Although in the results presented in this paper a simplified penalty function is used to obtain a first cut at the aero-structural design problem, we feel it is important to place the mathematical framework for coupled sensitivities on more solid footing. It will inevitably turn out that the choice of the use of an adjoint approach will depend upon the problem at hand. Since we propose to establish a flexible design environment, the possibility of using a coupled adjoint must be considered. The remainder of this section has been developed in collaboration with Lessoine [27].

Consider, for example, a cost function where both aircraft weight and drag are included. Then, if $\mathbf{q}$ and $\mathcal{P}$ denote respectively the structural displacement field and structural parameters of the structural model, $\mathbf{w}$ denotes the flow solution, and $\mathcal{F}$ represents the design parameters of the undeformed aircraft shape, the aeroelastic objective function whose sensitivity we are looking for becomes $I(\mathbf{w}, \mathbf{q}, \mathcal{F}, \mathcal{P})$. The variations in I are subject to the constraint

$$R_{as}(\mathbf{w}, \mathbf{q}, \mathcal{F}, \mathcal{P}) = 0, \tag{15}$$

where R_{as} designates the set of aero-structural equations and can be partitioned as

$$R_{as} = \begin{pmatrix} R(\mathbf{w}, \mathbf{q}, \mathcal{F}, \mathcal{P}) \\ S(\mathbf{w}, \mathbf{q}, \mathcal{F}, \mathcal{P}) \end{pmatrix}. \tag{16}$$

Here, R denotes the set of fluid equations and S the set of structural equations. The variation δI can be expressed as

$$\delta I = \frac{\partial I^T}{\partial \mathbf{w}}\delta\mathbf{w} + \frac{\partial I^T}{\partial \mathbf{q}}\delta\mathbf{q} + \frac{\partial I^T}{\partial \mathcal{F}}\delta\mathcal{F} + \frac{\partial I^T}{\partial \mathcal{P}}\delta\mathcal{P}. \tag{17}$$

In order to eliminate $\delta\mathbf{w}$ and $\delta\mathbf{q}$ from the above equation, the following constraint can be introduced:

$$\begin{aligned} \delta R_{as} \quad = \quad & \left[\frac{\partial R_{as}}{\partial \mathbf{w}}\right]\delta\mathbf{w} + \left[\frac{\partial R_{as}}{\partial \mathbf{q}}\right]\delta\mathbf{q} \\ & + \left[\frac{\partial R_{as}}{\partial \mathcal{F}}\right]\delta\mathcal{F} + \left[\frac{\partial R_{as}}{\partial \mathcal{P}}\right]\delta\mathcal{P} = 0, \end{aligned}$$

which calls for the partitioned Lagrange Multiplier

$$\psi_{as} = \begin{pmatrix} \psi_a \\ \psi_s \end{pmatrix}, \tag{18}$$

where ψ_a is the portion of the adjoint associated with the fluid, and ψ_s is the portion of the adjoint associated with the structure. It follows that the first expression of δI can be replaced by

$$\begin{aligned} \delta I &= \tfrac{\partial I^T}{\partial \mathbf{w}}\delta\mathbf{w} + \tfrac{\partial I^T}{\partial \mathbf{q}}\delta\mathbf{q} + \tfrac{\partial I^T}{\partial \mathcal{F}}\delta\mathcal{F} + \tfrac{\partial I^T}{\partial \mathcal{P}}\delta\mathcal{P} \\ &-\psi_{as}^T\left(\left[\tfrac{\partial R_{as}}{\partial \mathbf{w}}\right]\delta\mathbf{w} + \left[\tfrac{\partial R_{as}}{\partial \mathbf{q}}\right]\delta\mathbf{q} + \left[\tfrac{\partial R_{as}}{\partial \mathcal{F}}\right]\delta\mathcal{F} + \left[\tfrac{\partial R_{as}}{\partial \mathcal{P}}\right]\delta\mathcal{P}\right) \\ &= \left\{\tfrac{\partial I^T}{\partial \mathbf{w}} - \psi_{as}^T\left[\tfrac{\partial R_{as}}{\partial \mathbf{w}}\right]\right\}\delta\mathbf{w} + \left\{\tfrac{\partial I^T}{\partial \mathbf{q}} - \psi_{as}^T\left[\tfrac{\partial R_{as}}{\partial \mathbf{q}}\right]\right\}\delta\mathbf{q} \\ &+ \left\{\tfrac{\partial I^T}{\partial \mathcal{F}} - \psi_{as}^T\left[\tfrac{\partial R_{as}}{\partial \mathcal{F}}\right]\right\}\delta\mathcal{F} + \left\{\tfrac{\partial I^T}{\partial \mathcal{P}} - \psi_{as}^T\left[\tfrac{\partial R_{as}}{\partial \mathcal{P}}\right]\right\}\delta\mathcal{P}. \end{aligned}$$

Now, if ψ is chosen as the solution of the aero-structural adjoint equation

$$\begin{pmatrix} \left(\frac{\partial R_{as}}{\partial \mathbf{w}}\right)^T \\ \left(\frac{\partial R_{as}}{\partial \mathbf{q}}\right)^T \end{pmatrix}\begin{pmatrix} \psi_a \\ \psi_s \end{pmatrix} = \begin{pmatrix} \frac{\partial I}{\partial \mathbf{w}} \\ \frac{\partial I}{\partial \mathbf{q}} \end{pmatrix}, \tag{19}$$

the expression for δI simplifies to

$$\delta I = \mathcal{G}_{\mathcal{F}}\delta\mathcal{F} + \mathcal{G}_{\mathcal{P}}\delta\mathcal{P}, \tag{20}$$

where

$$\mathcal{G}_{\mathcal{F}} = \frac{\partial I^T}{\partial \mathcal{F}} - \psi_{as}^T\left[\frac{\partial R_{as}}{\partial \mathcal{F}}\right], \tag{21}$$

and

$$\mathcal{G}_{\mathcal{P}} = \frac{\partial I^T}{\partial \mathcal{P}} - \psi_{as}^T \left[\frac{\partial R_{as}}{\partial \mathcal{P}} \right]. \qquad (22)$$

Hence, the sought-after objective, which is the elimination of $\delta\mathbf{w}$ and $\delta\mathbf{q}$ from the expression for δI, is attainable but requires the solution of the adjoint *coupled aero-structural* problem

$$\begin{pmatrix} \left(\frac{\partial R}{\partial \mathbf{w}}\right)^T & \left(\frac{\partial S}{\partial \mathbf{w}}\right)^T \\ \left(\frac{\partial R}{\partial \mathbf{q}}\right)^T & \left(\frac{\partial S}{\partial \mathbf{q}}\right)^T \end{pmatrix} \begin{pmatrix} \psi_a \\ \psi_s \end{pmatrix} = \begin{pmatrix} \frac{\partial I}{\partial \mathbf{w}} \\ \frac{\partial I}{\partial \mathbf{q}} \end{pmatrix}. \qquad (23)$$

Now, since the creation of a completely coupled aero-structural adjoint would compromise our objective of developing a flexible MDO framework, we can rewrite Eq. (23) as

$$\begin{aligned} \left(\frac{\partial R}{\partial \mathbf{w}}\right)^T \psi_a &= \frac{\partial I}{\partial \mathbf{w}} - \left(\frac{\partial S}{\partial \mathbf{w}}\right)^T \tilde{\psi}_s \\ \left(\frac{\partial S}{\partial \mathbf{q}}\right)^T \psi_s &= \frac{\partial I}{\partial \mathbf{q}} - \left(\frac{\partial R}{\partial \mathbf{q}}\right)^T \tilde{\psi}_a, \end{aligned}$$

where $\tilde{\psi}_s$ and $\tilde{\psi}_a$ are lagged values which are updated via outer iterations. This implies that existing adjoint solvers for both the aerodynamics and structures can be used subject to convergence of the iteration. The additional right-hand-side forcing terms can then be updated in the same way as has been done here with the state equations. Thus, the OML geometry can serve to couple both the state and costate equations.

Beyond employing a coupled adjoint, the alternative of using a coupled direct approach also exists. The development follows the one above very closely in terms of the coupling. The terms in Eq. (12) which were assumed to be zero become the coupling variables. However, since prefactoring of the CFD Jacobian matrix is problematic, the approach will not be much cheaper than using finite differencing. An alternative to either the adjoint or the direct approaches is the use of a decomposed optimization strategy such as multi-level optimization [28] or collaborative optimization [15]. Exploring all of these various possibilities will form the basis of our future work.

For the purposes of the present paper where a coupled adjoint has yet to be implemented, the sensitivities are obtained without coupling. The aerodynamic adjoint is used to obtain aerodynamic sensitivities and finite differences are used to obtain the structural sensitivities. This approximation inherently implies that gradient information for a combined aerodynamic plus structural objective function will not be completely accurate. The earlier example of exploring how wing twist affects structural stress levels highlights our current limitation. Without the coupling, we will capture only the portions of the sensitivities that result from structural changes. The loading will act as if it were frozen just as in Eq. (12). Future works will address this limitation by implementing the coupled adjoint as outlined above. Finally, for a detailed treatment of the overall design process, we refer to references [5, 6].

6 Results

The results of the application of our aero-structural design methodology are presented in this section. These results are divided into two parts: results of aeroelastic analysis of existing complete configuration wind tunnel models, and results of aeroelastic design for flight configurations. The two sets of results use two different structural models. In addition, some of the results presented used the Euler equations, while others used the Reynolds Averaged Navier-Stokes equations to model the fluid flow. The results are intended to showcase the current capabilities of the design method.

6.1 Navier-Stokes Aeroelastic Analysis of Complete Configuration Wind Tunnel Models

In this section, results of the rigid and aeroelastic analysis of two different wind tunnel models representing typical complete configuration business jets are presented and compared with the available experimental data. The CFD meshes used for each of the two models contain the wing, body, pylon, nacelle, and empennage components. The mesh for the first model (model A) uses 240 blocks with a total of 5.8 million cells while the second mesh (model B) contains 360 blocks and a total of 9 million cells. The large mesh sizes are required for adequate resolution of all the geometric features for each of the configurations and the high Reynolds number boundary layers on their wings. It should be mentioned that viscous and structural effects are resolved only on the wing surface; all other surfaces in the model are assumed to be inviscid and rigid. All calculations were run using 48 processors of an SGI Origin2000 parallel computer. A total of 1.3 hours (model A) and 2.0 hours (model B) of wall clock time were required for the rigid-geometry solutions, while 1.4 hours and 2.1 hours were required for the aeroelastic calculations. The structural model is the one described in Section 3.1 since the properties of its elements more closely approximate the behavior of the wind tunnel model structure. Experimental wind tunnel data are available for the two models at flight conditions as follows: Model A, $M_\infty = 0.80$, $Re = 2.5$ million and cruise C_L, and Model B, $M_\infty = 0.80$, $Re = 2.4$ million and cruise C_L. Aeroelastic updates are performed every 10 multigrid iterations of the flow solver. A total of

400 iterations were used to ensure an aeroelastically converged solution. All solutions were calculated at a fixed C_L by incrementally adjusting the angle of attack.

A view of model A colored by C_p appears in Figure 4 showing the wing, body, pylon, nacelle, and empennage present in the calculation. Figure 5 shows a comparison of the pressure distributions for the rigid wing, the aeroelastic wing, and the wind tunnel data for model A. The sectional cut is near mid-span where wind tunnel measurements were available. The figure shows that for this case the aeroelastic deformation of the wing is so small that virtually no difference between the two computed results exists. In fact, the maximum tip deflection of the model was calculated to be only 0.3% of the wing span. Agreement with the sparse wind tunnel data indicates that the CFD is capturing the right trends present in the tested configuration. The fact that the differences between the computed rigid and elastic wings are so small leads to the conclusion that the wind tunnel data from this test probably need not be corrected for aeroelastic deflections. In retrospect, it can be noted that the model A configuration has low sweep so there is very little twist due to bending. Thus, since the outboard wing tip is not twisting much, large differences in the pressure distribution do not appear. If these calculations had been performed before test entry, the confidence level on the tunnel data could have been increased. Figure 6 shows the difference in the spanload of the two computed solutions.

Figure 7 shows a similar comparison of pressure distributions for rigid, aeroelastic, and wind tunnel data from model B. It is immediately clear that the deflections predicted by the aeroelastic calculation have a much larger impact on the pressure distributions than in the case of model A. The changes in the pressure distributions show all the typical signs of aeroelastic relief in swept-back wings: a decrease in the twist of the outboard sections of the wing with the consequent forward motion of the shock location and alterations in the spanload distribution.

Although the aeroelastic solution does not agree fully with the experimental data for model B, it is clear that the aerolastic effects change the solution in the correct direction to improve the agreement. Additional discrepancies are believed to be caused by inaccuracies in the Baldwin-Lomax turbulence model. It is also evident that this wind tunnel model is flexible enough that significant aeroelastic effects are present in the wind tunnel data. In view of the small increase in cost of the aeroelastic solutions, it is clear that this type of analysis is preferable for the comparison between experimental and wind tunnel data in order to eliminate some of the uncertainties causing the differences.

6.2 Aerodynamic Shape Optimization of a Flight Wing-Alone Geometry

The results presented in this section correspond to a typical aerodynamic shape optimization calculation on a rigid geometry. The structural model is completely inactive. This calculation is representative of many of our earlier works [5, 6] and is intended to present a baseline for comparison with aeroelastic designs in subsequent sections.

The geometry to be optimized is the wing of a typical business jet having the same planform as that of the airplane shown in Figure 4. The flow field is computed using the Euler equations. A multiblock mesh following a C-H topology is constructed around the configuration with a total of 32 blocks and $750,000$ cells. A total of 133 design variables are used to parametrize the surface of the wing. Hicks-Henne perturbation functions combined with exponential functions at the wing trailing edges were distributed across the entire span of the wing to provide full geometric flexibility. Thickness constraints typical of our previous works are imposed in order to maintain the structural soundness of the final outcome of the design process. These constraints include spar depth constraints at 10% and 80% chord, a leading edge radius constraint ahead of the 2% location, a trailing edge included angle constraint behind the 95% chord location, and an additional thickness constraint to maintain maximum thickness and fuel volume at 40% chord. Note once more that these thickness constraints are the results of low-fidelity analyses and are derived from years of accumulated experience by aerodynamic and structural designers. The objective function is the wing coefficient of drag, C_D, at a fixed cruise $C_L = 0.35$ and a fixed Mach number of $M = 0.82$. It must be said that these flight conditions represent a significant increase in both Mach number and lift coefficient over those for which the original baseline wing was designed. It is therefore expected that improved aerodynamic designs should be attainable with the use of optimization. All wing-alone design calculations presented hereafter were carried out on an SGI Origin2000 parallel computer using 16 processors.

The results of this single-point shape optimization process can be seen in Figure 8 which shows the initial and final pressure distributions for several span stations along the wing. Similar results have been presented in [12]. Notable features are the decrease in induced drag due to the shifting of the spanload towards the tip (Figure 9) and the decrease of wave drag that results from the weakening or disappearance of the shock waves on the upper and lower surfaces. Note that at the location of the front spar (10% chord) where the thickness constraint is active, the lower surface pressure distribution at some

of the stations exhibits an oscillation and a loss of lift due to the requirement of maintaining thickness. The changes in airfoil shape are rather small, but the overall effect on the C_D of the configuration is drastic: after 20 design iterations, the total value of C_D is reduced by 31%, or from 95.6 counts to 65.6 counts.

As shown in Figure 10, a comparison of aeroelastic analyses of the baseline and resulting designs reveals that the maximum stress levels for the rear spar have increased substantially in the inboard wing region, especially near the crank point. Figure 9 shows that the reason for the increase in stress in the rear spar is that the span loading has been shifted outboard substantially for this rigid-wing design in an effort to reduce the induced drag. Since the optimization algorithm can not see a structural penalty in this outboard shift of the spanload, it simply maintains the required thickness constraints and redistributes the load as it sees fit.

6.3 Aerodynamic Shape Optimization of a Flight Wing-Alone Geometry Including Aeroelastic Deformations

The design example presented in this section is identical to the one in the previous section with the only difference being that the structure is no longer assumed to be rigid. During the flow calculation process, the structural model is allowed to deform under aerodynamic loads. However, the cost function to be minimized still remains the coefficient of drag of the wing, C_D, and the same artificial thickness constraints are imposed on the problem. Since this design case constitutes only a small perturbation of the previous problem, it is expected that its outcome will differ from the last case by only a small amount. Indeed, this is the case: the resulting pressure distributions, as seen in Figure 11, are nearly identical across the span, with very similar changes in the aerodynamic shape when compared with Figure 8. However, an expected trend is seen when this design is compared with the former design analyzed aeroelastically. Because the rigid-wing design settled on a span loading that minimized induced drag while maintaining the geometric constraints in the rigid mode, it becomes less than optimum when it is analyzed in the presence of the aeroelastic relief. Meanwhile, the wing designed in the presence of aeroelastic effects will compensate for this washout and make the appropriate shift in the spanloading to optimize performance despite the increase in twist. This is precisely the effect that can be seen in Figure 12. Apart from this subtle difference, both designs are quite close to each other. Figure 13 depicts a comparison between the initial and final spanwise stress distributions on the rear spar showing the same trend of increased inboard stress near the crank point as was seen in the rigid-wing design case.

6.4 Aero-Structural Shape Optimization of a Flight Wing-Alone Geometry

The idea in this final wing-alone design case is to incorporate some basic elements of the aero-structural interaction present in the existing design methodology. Despite the fact that development of the complete coupled sensitivity analysis is not yet implemented, several results of interest can be shown which establish the soundness of the procedure. In this particular case, we utilize the geometry of the previous two sections, the same CFD mesh and structural model, and the same set of aerodynamic shape variables. The artificial thickness constraints are removed, leaving only the leading edge radius and included trailing edge angle constraints. The design is now set up with both the coefficient of drag and the $\mathcal{L}^2$ norm of the stress in the structure as a combined cost function. This combined penalty function method can be thought of as a first cut approach to minimizing total drag in the presence of structural constraints. The ASO adjoint system is used to calculate the gradient of the aerodynamic cost function (C_D) and finite differencing is used to calculate the gradient contribution from the structural changes. Despite the fact that these sensitivities are not fully accurate because of the lack of coupling, they provide our first approximation for solving the AESO (AeroElastic Shape Optimization) problem. The weights between the two components of the objective function were arbitrarily chosen such that the stress penalty was equal to about 40% of the drag penalty. This choice resulted in an optimized design where the $\mathcal{L}^2$ norm of the stress in the structure remained largely unchanged.

Figure 14 depicts the pressure distributions before and after the design process. Once more, the resulting pressure distributions and changes to the sections look similar to those from the previous two design cases. However, there are some noteworthy differences. The oscillation in the lower surface pressure distribution seen in the earlier two solutions near the 10% span chord location is not present. Since we are no longer imposing artificial thickness constraints, the resulting design was able to thin this region with some benefit to the aerodynamics and without a significant increase in the structural stress distributions. The more clearly observable difference between this solution and the previous two is the dramatic thickening of the airfoil section near the crank point. This is the location where the highest stress level is recorded in the rear spar. Figure 15 shows that the design has again

dramatically changed the loading distributions by moving part of the load outboard. This has a corresponding tendency to increase the load at the critical crank point rear spar location. The design algorithm has chosen to increase the airfoil thickness at this station to compensate for the shift in load outboard. It is worth remembering that changes to the wing thickness can have an effect on wave drag. Indeed a re-examination of Figure 14 reveals that the shock strength on the lower surface has been increased from the original design. However, since the final design in this case is less than one count higher in drag than that achieved in the previous two cases, this weak lower surface shock must not be incurring a significant drag penalty. Figure 16 illustrates the benefit of adding the stress penalty function to the design problem. The spanwise stress on the rear spar at the planform break has been reduced slightly in the optimized configuration. Assuming that no other constraints were placed on the problem, it would then be possible to shift the load on the wing outboard, while thickening the inboard sections so as to keep the wing weight approximately constant. With a more accurate description of the cost functions and constraints in the problem, these kinds of trade studies will allow the designer to make better-informed choices about the development of the configuration.

6.5 Aero-Structural Shape Optimization of a Wing in the Presence of a Complete Configuration

The final test case demonstrates the capability of the new design algorithm to treat complete aircraft configurations. The configuration modeled in the CFD analysis includes a wing, body, nacelle pylon and empennage. In this case the Euler equations were used to model the flow during the design process. The mesh for the configuration contains 240 blocks and 4.2 million cells. The structural model used in the previous three design cases is used again to obtain the structural deformations of the wing. The rest of the configuration is assumed to be rigid. The design conditions were chosen to be $M = 0.82$ and $C_L = 0.30$. These numbers, just as in the wing-alone design cases, represent an increase in the Mach number and lift coefficient over the design point for the initial configuration. Hence, it is expected that significant improvements to the drag should be realizable. The design calculations were carried out using 48 processors of an Origin2000.

The design approach follows that used for the last wing-alone design case: a combination of the drag coefficient and the $\mathcal{L}^2$ norm of the stresses in the structure is used as the objective function. The sensitivities are calculated separately using the adjoint for the aerodynamics and finite differences for the structures and neglecting the coupling between the two.

Figure 17 displays the airfoil sections and pressure distributions developed by the optimization procedure. It is evident that the optimized design has significantly reduced shock strengths, especially on the upper surface when compared with the baseline configuration. However, unlike the third wing-alone test case where we saw dramatic thickening of the lower surface of the configuration in the vicinity of the crank point in the planform, here only small changes are apparent. It is refreshing that no thickness constraints were necessary to ensure a realistic design and that the penalty function approach was sufficient to prevent the airfoil sections from becoming unreasonably thin. The differences between the result of this design and that of the wing-alone cases may seem at first puzzling. All of the geometry modifications were very slight for the case of the complete configuration. An examination of Figure 18 reveals a possible explanation: the loading distribution for the complete configuration was closer to the ideal distribution, and therefore there was not much to be gained from shifting the load to the outboard stations. Since the loading is not changing significantly, the required thickness changes near the crank point necessary to maintain reasonable stress levels (as can be seen in Figure 19) need not be drastic. The conclusion is that for this configuration the majority of the improvements in the aerodynamic performance (an 18.1% reduction in drag) are coming from a reduction in wave drag, and therefore the trade-off between aerodynamics and structures is not so significant.

7 Conclusions

The work presented in this paper represents our first step towards the establishment of a high-fidelity multidisciplinary environment for the design of aerospace vehicles. The environment is in its infancy and will continue to evolve during the coming year(s). At its core, it consists of the following key elements:

- High-fidelity modeling of the participating disciplines (RANS flow models for the aerodynamics and linear finite element model for the structure).
- An OML geometry database which serves as the interface between disciplines. This database contains information regarding the current shape of the configuration and the physical solutions from the participating disciplines.
- A force- and work-equivalent coupling algorithm designed to preserve a high level of accu-

racy in the transfer of loads and displacements between aerodynamics and structures.

- A framework for the computation of coupled sensitivities of the aero-structural design problem.

This design environment has been used to perform RANS aeroelastic analysis of complete configuration flight and wind-tunnel models with an additional cost which is less than 10% of the cost of a traditional rigid-geometry CFD solution. These solutions can be used to determine *a priori* whether significant aeroelastic corrections will or will not be needed for the resulting wind tunnel data.

In addition, simplified design cases have been presented that include the effect of aeroelastic deformations in the design process. These cases have shown that our design methodology is able to predict the correct trades between aerodynamic performance and structural properties present in these types of wing design problems.

Finally, a structural stress penalty function was added to the coefficient of drag of the complete configuration to allow elimination of artificial thickness constraints that are typically imposed in aerodynamic shape optimization methods. This rudimentary coupling of aerodynamics and structures in the design not only eliminates the necessity to impose artificial constraints, but also produces designs where trade-offs between aerodynamic and structural performance are considered.

Further work will focus on the continued development of the proposed MDO framework. Topics requiring significant research include sensitivity analysis, optimization strategy, Navier-Stokes based design, use of commercially available CSM codes, multipoint design, and CAD integration.

8 Acknowledgments

This research has been made possible by the support of the MCAT Institute, the Integrated Systems Technologies Branch of the NASA Ames Research Center under Cooperative Agreement No. NCC2-5226, and the David and Lucille Packard Foundation. Raytheon Aircraft is acknowledged for providing relevant aircraft configurations and wind tunnel data as well as guiding the overall research effort. The authors would like to acknowledge the assistance of David Saunders in the review of the final manuscript and the help of Mark Rimlinger in the preparation of CFD meshes and figures.

References

[1] J. Sobieszczanski-Sobieski and R. T. Haftka. Multidisciplinary aerospace design optimization: Survey of recent developments. *AIAA paper 96-0711*, 34th Aeospace Sciences Meeting and Exhibit, Reno, NV, January 1996.

[2] S. Wakayama. Lifting surface design using multidisciplinary optimization. *Ph. D. Dissertation*, Stanford University, Stanford, CA, December 1994.

[3] S. R. Wakayama and I. M. Kroo. A method for lifting surface design using nonlinear optimization. Dayton, OH, Sept. 1990. AIAA Paper 90-3120. AIAA/AHS/ASEE Aircraft Design Systems and Operations Conference.

[4] J. W. Gallman. *Structural and Aerodynamic Optimization of Joined-Wing Aircraft.* Ph.d. dissertation, Department of Aeronautics and Astronautics, Stanford University, Stanford, CA, June 1992.

[5] J. J. Reuther, A. Jameson, J. J. Alonso, M. Rimlinger, and D. Saunders. Constrained multipoint aerodynamic shape optimization using an adjoint formulation and parallel computers: Part I. *Journal of Aircraft*, 1998. Accepted for publication.

[6] J. J. Reuther, A. Jameson, J. J. Alonso, M. Rimlinger, and D. Saunders. Constrained multipoint aerodynamic shape optimization using an adjoint formulation and parallel computers: Part II. *Journal of Aircraft*, 1998. Accepted for publication.

[7] J. Reuther, A. Jameson, J. Farmer, L. Martinelli, and D. Saunders. Aerodynamic shape optimization of complex aircraft configurations via an adjoint formulation. *AIAA paper 96-0094*, 34th Aerospace Sciences Meeting and Exhibit, Reno, Nevada, January 1996.

[8] J. Reuther, A. Jameson, J. J. Alonso, M. J. Rimlinger, and D. Saunders. Constrained multipoint aerodynamic shape optimization using an adjoint formulation and parallel computers. *AIAA paper 97-0103*, 35th Aerospace Sciences Meeting and Exhibit, Reno, Nevada, January 1997.

[9] J. Reuther, J. J. Alonso, J. C. Vassberg, A. Jameson, and L. Martinelli. An efficient multiblock method for aerodynamic analysis and design on distributed memory systems. *AIAA paper 97-1893*, June 1997.

[10] A. Jameson, N. Pierce, and L. Martinelli. Optimum aerodynamic design using the Navier-Stokes equations. *AIAA paper 97-0101*, 35th Aerospace Sciences Meeting and Exhibit, Reno, Nevada, January 1997.

[11] A. Jameson. Re-engineering the design process through computation. *AIAA paper 97-0641*, 35th Aerospace Sciences Meeting and Exhibit, Reno, Nevada, January 1997.

[12] J. Reuther and A. Jameson. Aerodynamic shape optimization of wing and wing-body configurations using control theory. *AIAA paper 95-0123*, 33rd Aerospace Sciences Meeting and Exhibit, Reno, Nevada, January 1995.

[13] A. Jameson. Automatic design of transonic airfoils to reduce the shock induced pressure drag. In *Proceedings of the 31st Israel Annual Conference on Aviation and Aeronautics, Tel Aviv*, pages 5–17, February 1990.

[14] A. Jameson. Aerodynamic design via control theory. *Journal of Scientific Computing*, 3:233–260, 1988.

[15] I. M. Kroo. Decomposition and collaborative optimization for large scale aerospace design. In N. Alexandrov and M. Y. Hussaini, editors, *Multidisciplinary Design Optimization: State of the Art*. SIAM, 1996.

[16] R. Braun, P. Gage, I. Kroo, and I. Sobieski. Implementation and performance issues in collaborative optimization. *AIAA paper 96-4017*, 6th AIAA/USAF/NASA/ISSMO Symposium on Multidisciplinary Analysis and Optimization, Bellevue, WA, September 1996.

[17] A. Jameson and J.J. Alonso. Automatic aerodynamic optimization on distributed memory architectures. *AIAA paper 96-0409*, 34th Aerospace Sciences Meeting and Exhibit, Reno, Nevada, January 1996.

[18] A. A. Giunta, V. Balabanov, D. Haim, B. Grossman W. H. Mason, and L. T. Watson. Wing design for a high-speed civil transport using a design of experiments methodology. *AIAA paper 96-4001*, 6th AIAA/NASA/ISSMO Symposium on Multidisciplinary Analysis and Optimization, Bellevue, WA, September 1996.

[19] R. S. Sellar and S. M. Batill. Concurrent subspace optimization using gradient-enhanced neural network approximations. *AIAA paper 96-4019*, 6th AIAA/NASA/ISSMO Symposium on Multidisciplinary Analysis and Optimization, Bellevue, WA, September 1996.

[20] S. A. Brown. Displacement extrapolation for CFD+CSM aeroelastic analysis. *AIAA paper 97-1090*, 35th Aerospace Sciences Meeting and Exhibit, Reno, NV, January 1997.

[21] M. Holden. Optimization of dynamic systems using collocation methods. *Ph. D. Dissertation*, Stanford University, Stanford, CA, February 1999.

[22] R. Haimes. *CAPRI: Computational Analysis PRogramming Interface*. Massachusetts Institute of Technology, March 1998.

[23] R. M. Hicks and P. A. Henne. Wing design by numerical optimization. *Journal of Aircraft*, 15:407–412, 1978.

[24] R. Kennelly. Improved method for transonic airfoil design-by-optimization. *AIAA paper 83-1864*, AIAA Applied Aerodynamics Conference, Danvers, Massachusetts, July 1983.

[25] G. W. Burgreen and O. Baysal. Three-dimensional aerodynamic shape optimization of wings using sensitivity analysis. *AIAA paper 94-0094*, 32nd Aerospace Sciences Meeting and Exhibit, Reno, Nevada, January 1994.

[26] H. M. Adelman and Raphael T. Haftka. Sensitivity analysis of discrete structural systems. *AIAA Journal*, 24:823–832, 1986.

[27] J. Gallman, J. J. Alonso, J. Reuther, and M. Lessoine. Multi-disciplinary optimization using computational fluid dynamics (cfd). Topic Area Number 29: BAA 98-04-PRK, Research Proposal Submitted to the Air Force Research Laboratory, Wright-Patterson Airforce Base, Dayton, Ohio, 1998.

[28] M. Baker and J. Giesing. A practical approach to mdo and its application to an hsct aircraft. *AIAA paper 95-3885*, 1st AIAA Aircraft Engineering, Technology, and Operations Congress, Los Angeles, CA, September 1995.

Figure 4: Typical business jet configuration. FLO107-MB: Navier-Stokes, Baldwin-Lomax, $M = 0.80$, $Re =$ 2.5 million, 5.8. million mesh cells. C_p contours.

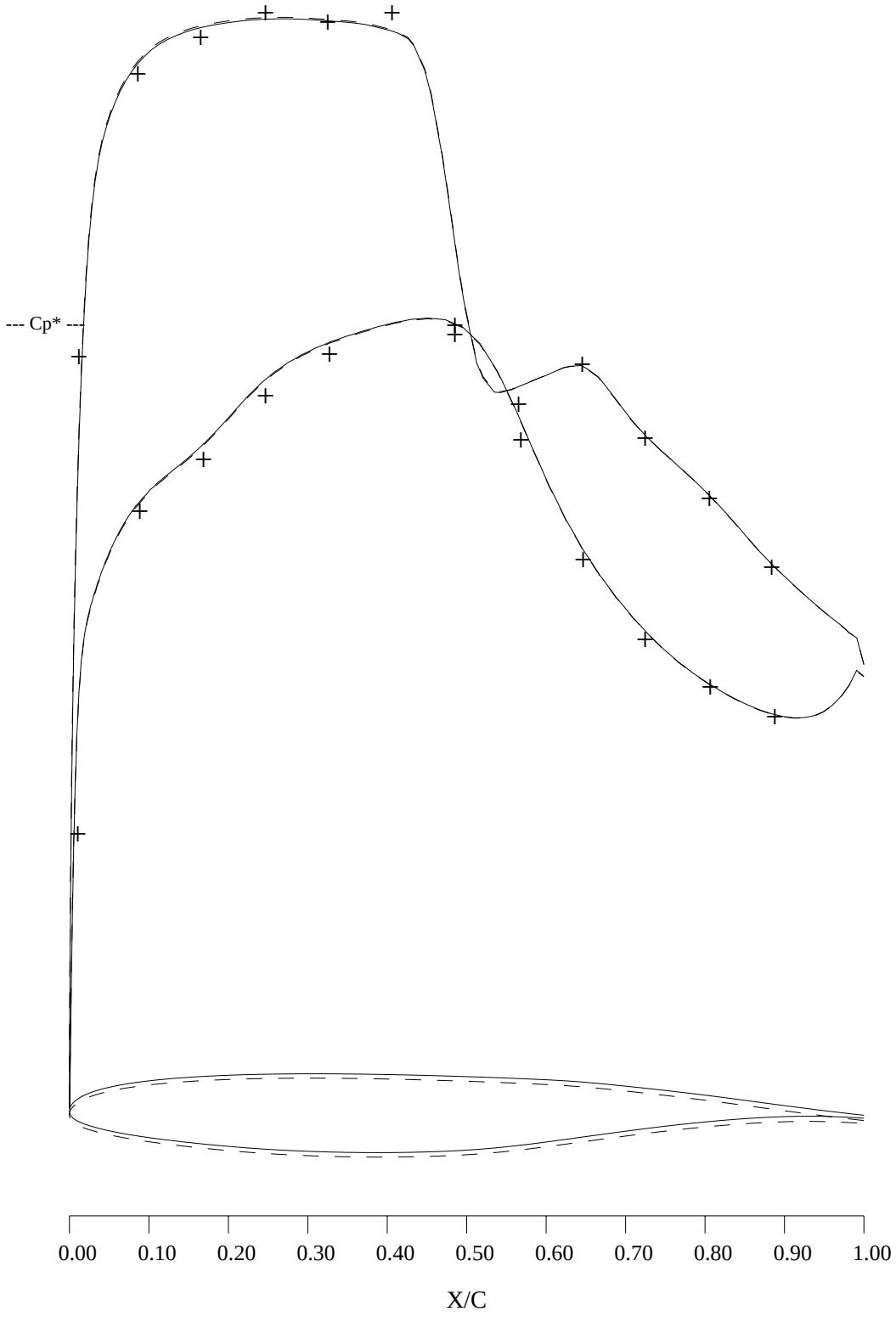

Figure 5: C_p distribution at near wing tip station. Navier-Stokes calculations, $M = 0.80$, $Re = 2.5$ million
———, Aeroelastic solution
– – –, Solid geometry solution
+ + +, Wind tunnel data

Figure 6: Spanwise Load Distribution.
Comparison of the Rigid Analysis and Aeroelastic Analysis.
Complete Configuration Navier-Stokes Solution.

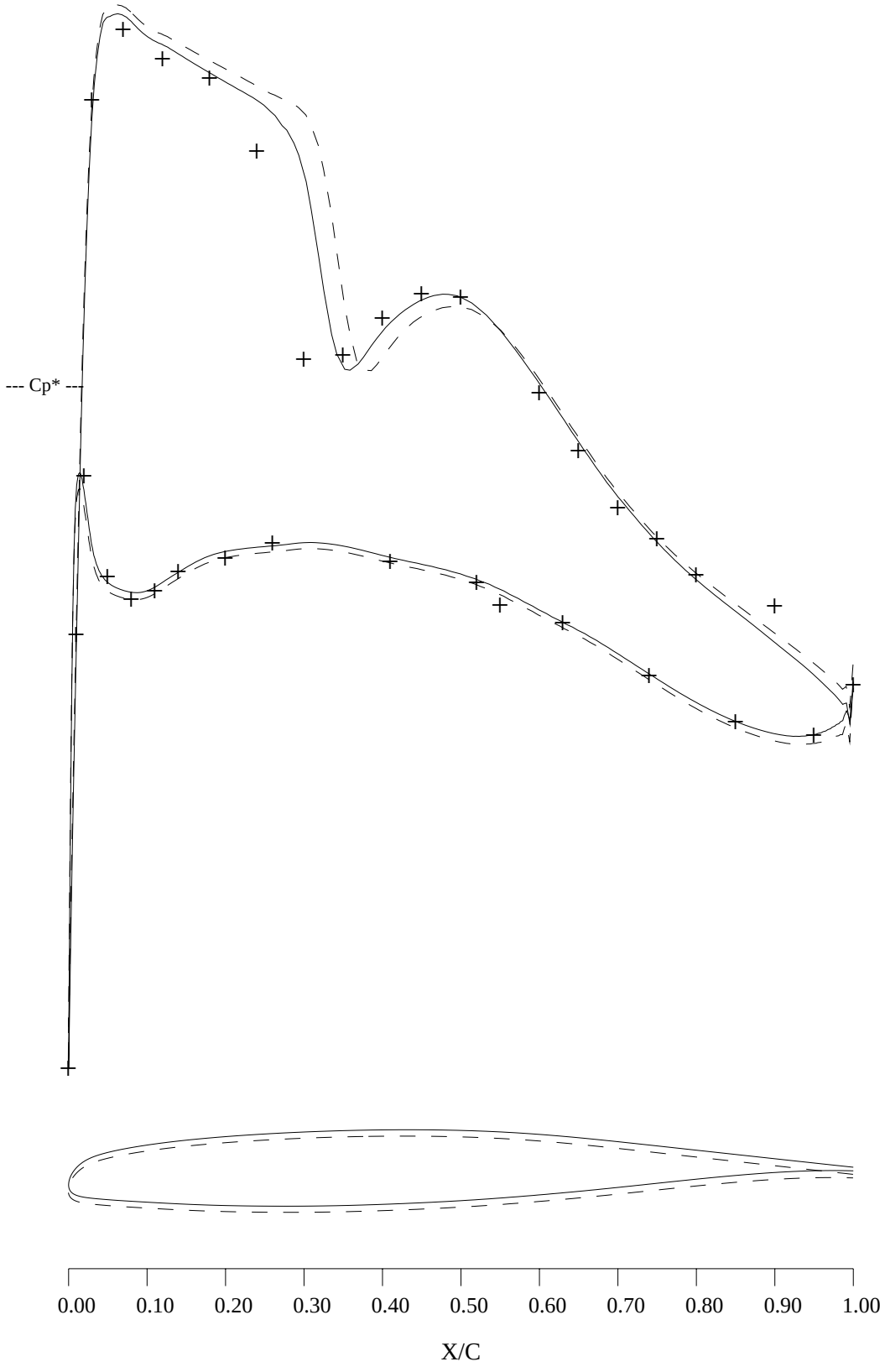

Figure 7: C_p distribution at near wing tip station. Navier-Stokes calculations, $M = 0.80$, $Re = 2.4$ million
———, Aeroelastic solution
– – –, Solid geometry solution
+ + +, Wind tunnel data

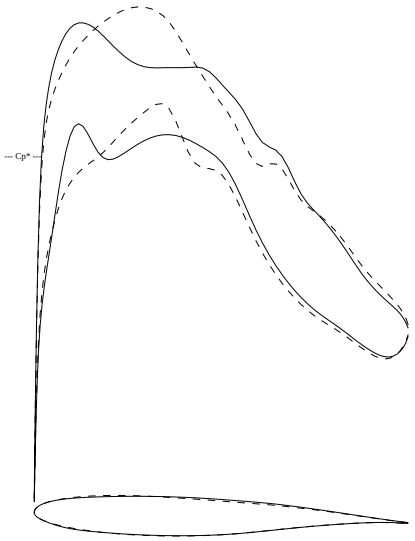

8a: span station $z = 0.194$

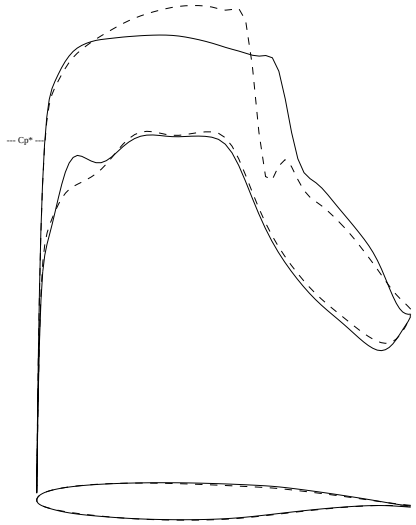

8b: span station $z = 0.387$

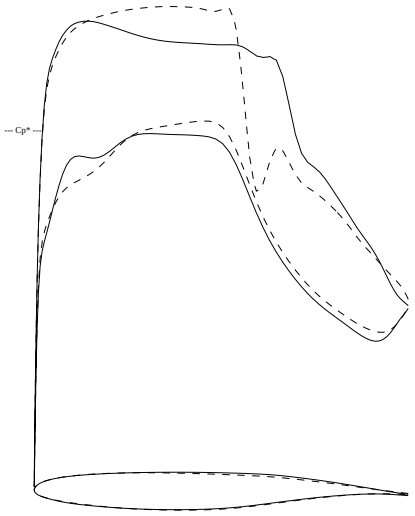

8c: span station $z = 0.581$

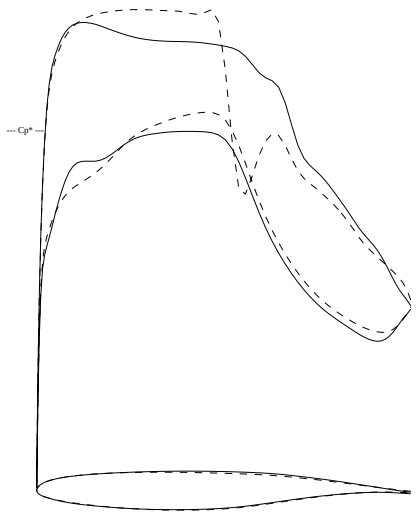

8d: span station $z = 0.775$

Figure 8: Typical Business Jet Configuration. Drag Minimization at Fixed C_L.
Rigid Design, $M = 0.82$, $C_L = 0.35$, 133 Hicks-Henne variables. Spar Constraints Active.
Rigid Analysis at Fixed C_L.
– – –, Initial Pressures
———, Pressures After 20 Design Cycles.

Figure 9: Spanwise Load Distribution.
Comparison of the Rigid Design and the Baseline Design.
Wing Alone Configuration.
Rigid Design, Drag Minimization at Fixed C_L.
Aeroelastic Analysis at Fixed C_L.

Figure 10: Spanwise Stress Distribution for the Rear Spar.
Comparison of the Rigid Design and the Baseline Design.
Wing Alone Configuration.
Rigid Design, Drag Minimization at Fixed C_L.
Aeroelastic Analysis at Fixed C_L.

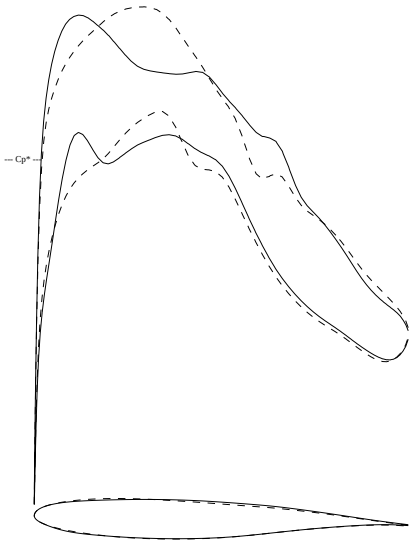

11a: span station $z = 0.194$

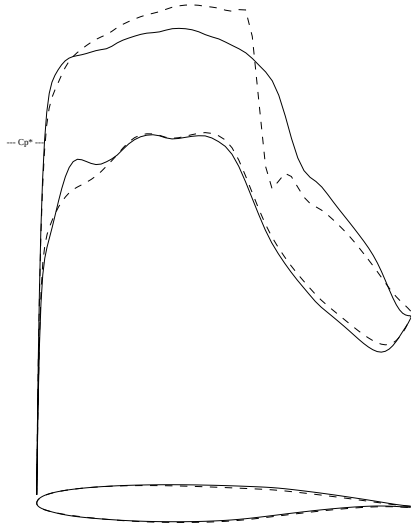

11b: span station $z = 0.387$

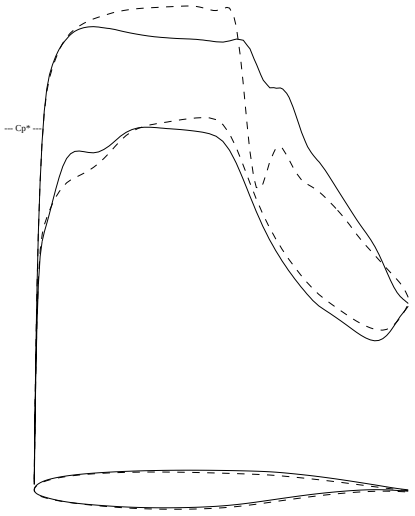

11c: span station $z = 0.581$

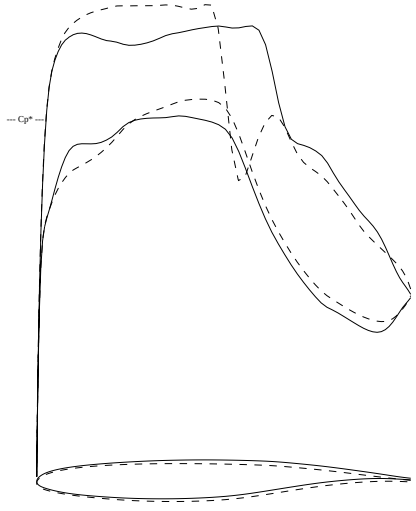

11d: span station $z = 0.775$

Figure 11: Typical Business Jet Configuration. Drag Minimization at Fixed C_L.
Design in the Presence of Aeroelastics. $M = 0.82$, $C_L = 0.35$
133 Hicks-Henne variables. Spar Constraints Active.
Aeroelastic Analysis at Fixed C_L.
– – –, Initial Pressures
———, Pressures After 13 Design Cycles.

Figure 12: Spanwise Load Distribution.
Comparison of the Aeroelastic Design and the Rigid Design.
Wing Alone Configuration.
Design in the Presence of Aeroelastics, Drag Minimization at Fixed C_L.
Aeroelastic Analysis at Fixed C_L.

Figure 13: Spanwise Stress Distribution for the Rear Spar.
Comparison of the Aeroelastic Design and the Rigid Design.
Wing Alone Configuration.
Design in the Presence of Aeroelastics, Drag Minimization at Fixed C_L.
Aeroelastic Analysis at Fixed C_L.

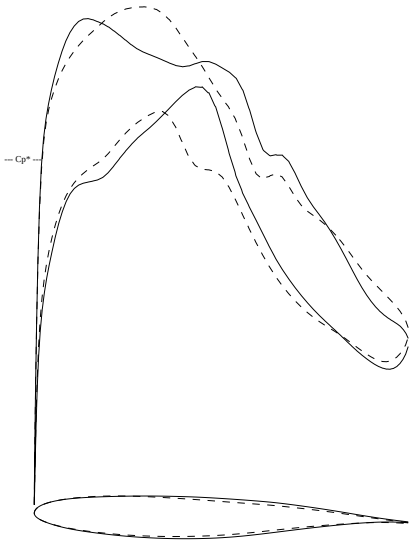

14a: span station $z = 0.194$

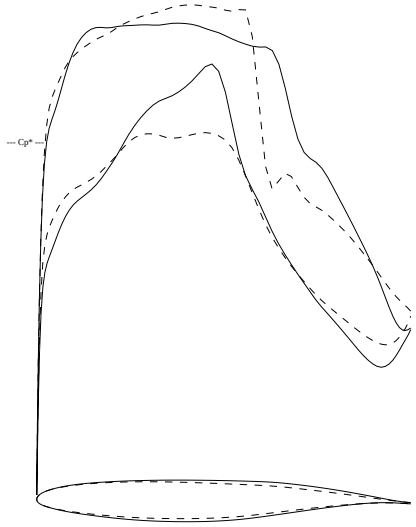

14b: span station $z = 0.387$

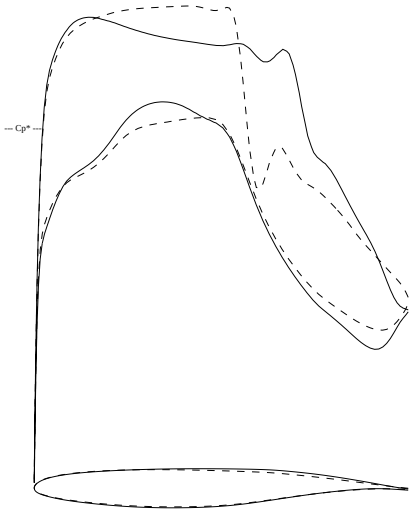

14c: span station $z = 0.581$

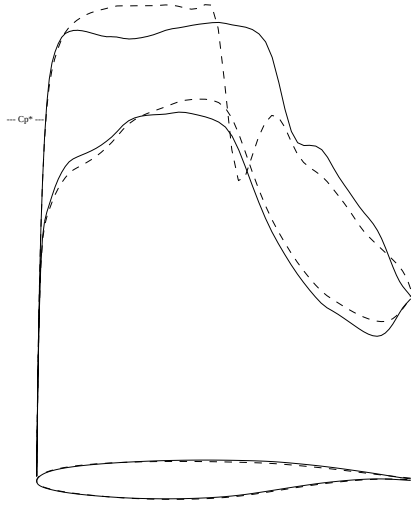

14d: span station $z = 0.775$

Figure 14: Typical Business Jet Wing Configuration. Drag + Stress Minimization at Fixed C_L.
Aeroelastic Design with Stress Penalty Function. $M = 0.82$, $C_L = 0.35$
133 Hicks-Henne variables. Spar Constraints Inactive.
Aeroelastic Analysis at Fixed C_L.
– – –, Initial Pressures
———, Pressures After 13 Design Cycles.

Figure 15: Spanwise Load Distribution.
Comparison of the Aeroelastic Design and the Rigid Design.
Wing Alone Configuration.
Aeroelstic Design, Drag + Stress Minimization at Fixed C_L.
Aeroelastic Analysis at Fixed C_L.

Figure 16: Spanwise Stress Distribution for the Rear Spar.
Comparison of the Aeroelastic Design and the Rigid Design.
Wing Alone Configuration.
Aeroelstic Design, Drag + Stress Minimization at Fixed C_L.
Aeroelastic Analysis at Fixed C_L.

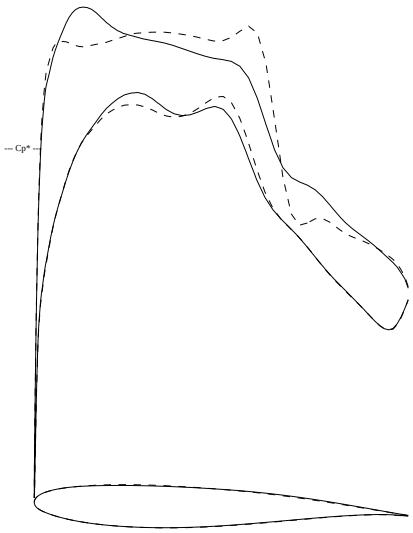

17a: span station $z = 0.194$

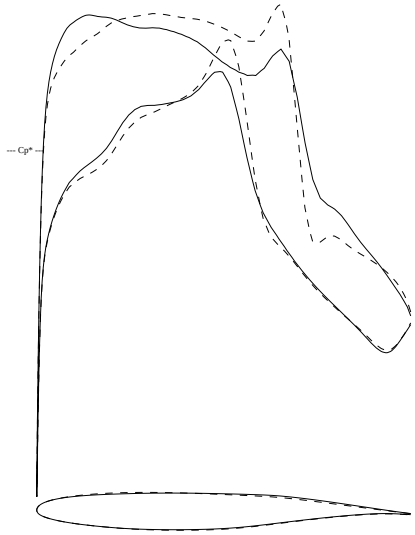

17b: span station $z = 0.387$

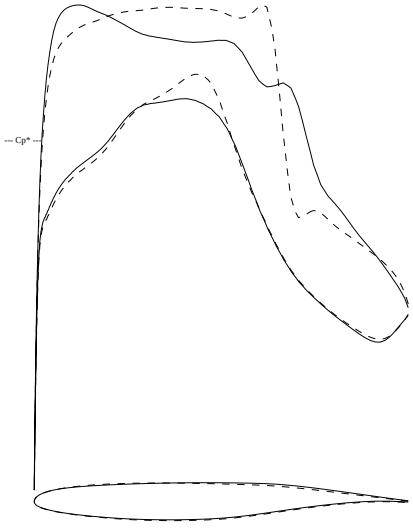

17c: span station $z = 0.581$

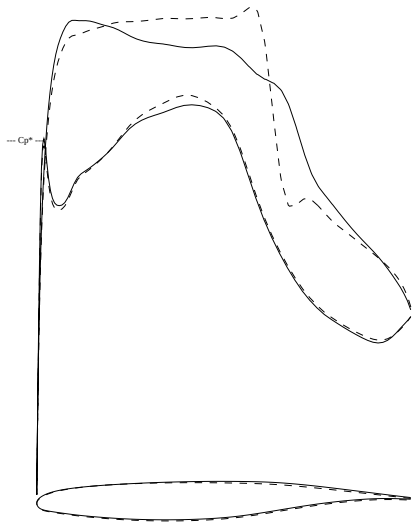

17d: span station $z = 0.775$

Figure 17: Typical Business Jet Full Configuration. Drag + Stress Minimization at Fixed C_L.
Aeroelastic Design with Stress Penalty Function. $M = 0.82$, $C_L = 0.30$
133 Hicks-Henne variables. Spar Constraints Inactive.
Aeroelastic Analysis at Fixed C_L.
– – –, Initial Pressures
———, Pressures After 7 Design Cycles.

Figure 18: Spanwise Load Distribution.
Comparison of the Aeroelastic Design and the Baseline.
Complete Configuration.
Aeroelastic Design, Drag + Stress Minimization at Fixed C_L.
Aeroelastic Analysis at Fixed C_L.

Figure 19: Spanwise Stress Distribution for the Rear Spar.
Comparison of the Aeroelastic Design and the Baseline.
Complete Configuration.
Aeroelastic Design, Drag + Stress Minimization at Fixed C_L.
Aeroelastic Analysis at Fixed C_L.